Assimilating High-resolution Sea Surface Temperature Data Improves the Ocean Forecast Potential in the Baltic Sea

Ye Liu[1], Weiwei Fu[2]

1. Swedish Meteorological and Hydrological Institute, Norrköping 60176, Sweden.

2. Department of Earth System Science, University of California, Irvine, California, 92697, USA.

Correspondence to: Ye Liu (ye.liu@smhi.se)

Abstract. We assess the impact of assimilating the satellite sea surface temperature (SST) data on the Baltic forecast, practically on the forecast of ocean variables related to SST. For this purpose, a multivariable DA system has been developed based on a Nordic version of the Nucleus for European Modelling of the Ocean (NEMO-Nordic). We use a Kalman-type filtering to assimilate the observations in the coastal regions. Further, a low rank approximation of the stationary background error covariance metrics is used at the analysis steps. High resolution SST from OSISAF is assimilated to verify the performance of DA system. The assimilation run shows very stable improvements of the model simulation as compared with both independent and dependent observations. The SST prediction of NEMO-Nordic is significantly enhanced by the DA system. Temperatures are also closer to observation in the DA system than the model results in the water above 100 m in the Baltic Sea. In the deeper layers, salinity is also slightly improved. Besides, we find that Sea level anomaly (SLA) is improved with the SST assimilation. Comparison with independent tide gauge data show that overall root mean square error (RMSE) is reduced by 1.8% and overall correlation coefficient is slightly increased. Moreover, the sea ice concentration forecast is improved considerably in the Baltic proper, the Gulf of Finland and the Bothnian Sea during the sea ice formation period, respectively.

1. Introduction

Monitoring the marine status of the Baltic Sea with relevant resolution and accuracy is a key requirement to serve the marine policy for detecting the influence of human activities on the environment and better understanding the response of ocean to accelerating global climate change. The Baltic Sea is one of the largest brackish seas in the world. It is a semi-enclosed basin, whose hydrography is highly variable and influenced by large-scale atmospheric processes and significant influx of freshwater from rivers runoff and precipitation (Leppäranta and Myrberg, 2009). In addition, the water exchange between the North Sea and Baltic Sea through the Danish straits is hindered by shallow topographic restrictions in the transition zone (Fig. 1).

A characteristic feature of numerical forecast in the Baltic Sea is in itself a major challenge because of complex topography and rich dynamics. A number of ocean forecasting systems for the Baltic Sea have been developed using hydrological model by operational agencies around this region. Traditionally, these models have a horizontal resolution of 1–5 km and approximately 20–100 layers in vertical structure (Omstedt et al. 2014). Due to the geographic location and conditions of the Baltic Sea, even higher resolutions are often needed to better understand the circulation dynamics. However, even ocean circulation models with a particularly high spatial resolution (e.g. 1 km) cannot resolve all dynamically important physical processes in the ocean (Malanotte-Rizzoli and Tziperman, 1996). In general, the forecast quality for a numerical model depends on initial conditions, boundary conditions (lateral, open boundaries as well as meteorological forcing and bathymetry) and a robust numerical model itself. As an operational forecasting agency, the Swedish Meteorological and Hydrological Institute's (SMHI) needs to issue well-informed forecasts and warnings for decision making by other authorities during e.g. severe weather events, but also to the public. To improve the forecast quality, the core three-dimensional dynamic model of the SMHI operational forecast system has recently migrated to the Nordic version of the Nucleus for European Modelling of the Ocean (NEMO-Nordic).

In additional to model development, an extended observational network has been established by the joint efforts of the countries surrounding the Baltic Sea. The observation platforms include vessels, buoys, coastal stations, satellite, etc. Specially, the observations from satellite have dominated the

53   coverage of SST observational networks in the Baltic Sea (She et al. 2007). Among satellite products,

54   the SST is most popularly and widely used for the operational forecast, reanalysis or validation of the

55   model because of both its coverage and properties. SST acts as a medium between atmospheric and

56   oceanic variations through activation of coupling mechanisms. SST is also a key ocean variable to link

57   many processes that occur in the upper ocean, for example, air-sea exchange of energy, primary

58   productivity, and formation of water masses (Tranchant et al., 2008).

59   A realistic forecast of SST is essential to an ocean forecasting system. SST is especially im-

60   portant for the Baltic Sea that the average water depth is only 56 m and its surface water is directly

61   related to the bottom water by the mixing in the shallow sub-basins. Recently, the applications of SST

62   for forecasting and analyzing the status of the North Sea and Baltic Sea have received particular atten-

63   tion. In the short-term forecast, Losa et al. (2012, 2014) investigated the systematic model uncertain-

64   ties for forecasting the North and Baltic Seas by assimilating the Advanced Very High Resolution

65   Radiometer (AVHRR) SST data. Nowicki et al. (2015) applied SST observed from Aqua Moderate

66   Resolution Imaging Spectroradiometer (MODIS) into 3D coupled ecosystem model of the Baltic Sea

67   with the Cressman analysis scheme. O'Dea et al. (2016) enhanced the SST prediction skill of the oper-

68   ational system by assimilating both in-situ data and level 2 SST data provided by the Global Ocean

69   Data Assimilation Experiment High-Resolution SST (GHRSST) into a European North-West shelf

70   operational model. Moreover, SST has been used in the long-term analysis in this region. For instance,

71   Stramska and Bialogrodzka (2015) analyzed spatial and temporal variability of SST in the Baltic sea

72   based on 32-years of satellite data, which indicate that there is a statistically significant trend of in-

73   creasing SST in the entire Baltic sea. However, these long-term SST data haven't been used to verify

74   the application of sophisticated DA methods for hydrography model in the Baltic profiles simulation,

75   especially at the Baltic deep water regions. Another important question is: what amount of satellite

76   SST can improve long-term forecast of ocean variables related to SST in the Baltic Sea.

77   The objective of this study is to address the impact of assimilating a high resolution SST product

78   on the forecast of the Baltic Sea, particularly the forecast of SST related variables like sea level and

79   sea ice. It is also the first time that satellite SST from the Ocean and Sea Ice Satellite Application Fa-

80   cility (OSISAF) was assimilated into NEMO-Nordic model (NEMO variant for the North Sea and

81   Baltic Sea). For operational forecast, the SST from OSISAF is the most important dataset in the Baltic

82   Sea because it differs from hindcast analyzed product like OSTIA (Operational SST and Sea Ice Anal-

83   ysis) data. As a level 2 product, the OSISAF SST has both good temporal and spatial coverage in the

84   Baltic Sea. As there is no hindcast information included in the OSISAF SST, we are able to assess

85   direct impacts of assimilating SST observations. Therefore, exploring the potential of this product is

86   critically important to further improving the new operational forecast system. In addition, our study

87   will enrich the reanalysis database of the Baltic Sea. In this study, we use the Singular Evolutive Inter-

88   polated Kalman (SEIK) filter (Pham, 2001) to account for the model uncertainties arising from a wide

89   range of spatial and temporal scales (Haines, 2010). One of our focuses is the impact of SST on the

90   modeled sea level and the sea ice in the Baltic Sea. For the whole Baltic Sea, how the SST assimila-

91   tion influences the temperature and salinity (T/S) on the different depth is another focus of this study.

92   The outline of the paper is as follows: the model configuration and SEIK scheme are described

93   in Section 2. An overview of the observations used in this study is presented in Section 3. The imple-

94   mentation of DA experiment is given in section 4 together with the sampling of ensemble and localiza-

95   tion. Results are compared with observations for temperature, salinity, sea level anomaly and sea ice in

96   Section 5. In this section, the impact of data assimilation on the forecasts is also investigated. Conclu-

97   sions and discussions are given in section 6.

98

2. Methodology

2.1 NEMO-Nordic

101   NEMO (Nucleus for European Modelling of the Ocean; Madec, 2008) has been set up at SMHI

102   for the North Sea and the Baltic Sea, a configuration called NEMO-Nordic (Hordoir et al., 2015) (Fig.

103   1). Open boundaries are implemented in northern North Sea between Scotland and Norway and in the

104   English Channel between Brittany and Cornwall, respectively (Hordoir et al., 2013). In this study,

105   NEMO-Nordic employs a horizontal resolution of 2 nautical miles (3.7 km) and 56 vertical levels, and

106   with a vertical resolution of 3 m close to the surface, decreasing to 22 m at the bottom of the deepest

107   part of the Norwegian trench. NEMO-Nordic uses a fully nonlinear explicit free surface (Adcroft and

108 Campin, 2004). A bulk formulation is used for the surface boundary condition (Large and Yeager,

109 2004). The ocean model is coupled to the Louvain-la-Neuve Sea Ice Model (LIM3) sea ice model

110 (Vancoppenolle et al., 2008) with a constant value of 10^{-3} PSU for the sea-ice salinity. A time-splitting

111 approach is used to compute a barotropic and a baroclinic mode, as well as the interaction between

112 them. A Tidal Inversion Model is used to define the barotropic mode at the open boundary conditions

113 (Egbert and Erofeeva, 2002). 11 tidal harmonics are defined for sea level and barotropic tidal veloci-

114 ties. In addition, a coarse resolution barotropic storm surge model covering a large area of the North-

115 ern Atlantic basin provides wind-driven sea level that is added to the tidal contribution. The T/S data

116 at the open boundary are provided by the Levitus climatology (Levitus and Boyer, 1994). Radiation

117 conditions are applied to calculate baroclinic velocities at these boundaries. A quadratic friction is

118 applied with a constant bottom roughness of 3 cm, and the drag coefficient is computed for each bot-

119 tom grid cell. NEMO-Nordic uses a TVD advection scheme with a modified leapfrog approach that

120 ensures a very high degree of tracer conservation (Leclair and Madec, 2009). Unresolved vertical tur-

121 bulence is parameterized with κ-ε scheme (Umlauf and Burchard, 2003). In addition, Galperin pa-

122 rameterization is used to obtain a stable long-term stratification for the Baltic Sea (Galperin et al.,

123 1988).

124   A Laplacian isopycnal diffusion is used for both momentum and tracers with a diffusion parame-

125 ter that is constant in time, but varies in space. Additional strong isopycnal diffusion is used close to

126 the Neva river inflow (Gulf of St. Petersburg) in order to avoid negative salinities. The bottom bound-

127 ary layer is parameterized to ease the propagation of saltwater inflows between the Danish Straits and

128 the deepest layers of the Baltic Sea (Beckmann and Doscher, 1997). A free-slip option is used for lat-

129 eral boundaries.

130   The model is forced by meteorological forcing derived from a downscaled run of Euro4M reanaly-

131 sis (Dahlgren et al., 2014). The downscaling is based on the regional atmospheric model RCA4 (Sam-

132 uelsson et al., 2011) which uses the reanalysis data as boundary conditions. A runoff database provides

133 the river flow to NEMO-Nordic (Donnelly et al. 2016); it includes inter-annual variability for the Bal-

134 tic Sea basin and is based on climatological values for the North Sea basin. The salinity of the river

135 runoff is set to a constant value of 10^{-3} PSU, which is the same value used for the sea-ice to avoid any

136   negative salinity.

137

138   **2.2 Local Sigular Evolutive Interpolated Kalman (LSEIK) filter**

139   The method used to assimilate SST into NEMO-Nordic is the Local Singular Evolutive Interpo-

140   lated Kalman (LSEIK) filter (Pham et al., 2001, Nerger et al. 2006). This is a sequential data assimila-

141   tion scheme, which is an error subspace extend Kalman filter that uses a minimum number of ensem-

142   ble members to reduce the prohibitive computation burden (Pham, 2001). The LSEIK filter produces

143   the correction for the model state by weighting the difference between the observations and the model

144   state estimation. The weight coefficients are constructed by the model error covariance matrix and

145   observation error covariance matrix. Similar as other ensemble-based data assimilation methods, the

146   LSEIK filter uses the spread of sample ensemble to estimate the uncertainties of the model state. Fur-

147   ther, a forgetting factor ρ is introduced to parameterize the imperfect model by amplifying the already

148   existing modes of the background error (Pham et al. 1998; Pham, 2001). Furthermore, the LSEIK filter

149   is based on an explicit low-rank approximation of the model error covariance matrix. A second-order

150   exact sampling method is used to initialize the LSEIK filter (Pham, 2001). Localization was also used

151   to remove the unrealistic long-range correlation with a quasi-Gaussian function and a uniform hori-

152   zontal correlation scale (Liu et al. 2013). It was performed by neglecting observations that were be-

153   yond correlation distance from an analyzed grid point. In other words, only data located in the "neigh-

154   borhood" of an analyzed grid point should contribute to the analysis at this point (Liu et al. 2009; Jan-

155   jić et al. 2011).

156

157   # 3. Observations

158   **3.1 Satellite observations**

159   The satellite SST used in DA was provided by OSISAF (http://osisaf.met.no/p/sst/index.html).

160   OSISAF aim is to produce, control and distribute operationally in near real-time products using avail-

161   able satellite data. The satellite datasets product used here includes the observations from polar orbit-

162   ing satellites (the EUMETSAT MetOp-A and NOAA-18, -19) with the AVHRR instrument. The SST

163   product has a resolution of 5 km and is produced twice daily at 00 UTC and 12 UTC. It covers the

164   Atlantic Ocean from 50°N to 90°N. The SST observations are thermal infrared observations from the

165   AVHRR instrument and are therefore limited by cloud cover (Kilpatrick et al. 2001). The cloud mask

166   in use is based on a multi-spectral thresholding algorithm by SMHI. The products were retrieved using

167   a nonlinear split window algorithm (Walton et al. 1998). The coefficients in the retrieval algorithm are

168   determined through regression toward in situ observations, and the dataset thus represents the subskin

169   temperature of the oceans. Further, subskin observations are subject to diurnal warming effects, which

170   can be significant in the Baltic Sea. Here only the subskin SST at night (00 UTC), which is compara-

171   ble to in situ (buoy) measurement, is used to minimum this effect. The SST is controlled with the cli-

172   matology check. A quality level from 0 to 5 is associated with every pixel. The higher level value, the

173   better the quality of the observations (Brisson et al., 2001). Observations with quality level 4 (good) or

174   5 (excellent) are collected for the analysis and low quality observations were removed. By applying

175   the above quality control processes, only a subset of the original OSISAF products is kept in this

176   study. Based on the former validation, a bias value of 0.5°C is given for this product.

177   Further, the IceMap from a sea ice concentration dataset with a high spatial resolution of 5 km

178   (http://www.smhi.se/oceanografi/iceservice/is_prod_en.php) is used to validate the DA results. It is

179   produced by SMHI and originates from digitized ice charts. An advantage of this data is that the ice

180   charts are quality checked manually. However, the drawback is that they include some subjective

181   steps. The temporal resolution of the IceMap SST is twice a week in the experiment period. Sea ice

182   occurs most frequently in the Bay of Bothnia, with up to 100 ice covered days per year. However, sea

183   ice can occur in all parts of the Baltic Sea and Danish straits, demonstrating the need for careful treat-

184   ment of sea ice in the SST analysis.

185

186   **3.2 In situ data**

187   The observations from the German Maritime and Hydrographic Agency (BSH) moored buoy

188   stations were collected as independent dataset to validate the assimilation results. The observations

189   have high temporal resolution and long continuous record. The second dataset was downloaded from

190   the Swedish Oceanographic Data Centre -SHARK database (http://sharkweb.smhi.se). SHARK mainly

191 contains low-resolution CTD data from a list of predefined standard stations in the Baltic Sea, as well

192 as in Kattegat and Skagerrak. Only observations that have passed gross quality control procedures are

193 collected into the SHARK database. This procedure includes, for example, location checks and local

194 stability checks. In addition, validating data records from tide gauges are also used. The sea level

195 anomaly measurements from tide gauges (sea level stations) are measured in a local height system and

196 values are presented relative to theoretical mean sea level, a level calculated from many years of annu-

197 al means, which takes into account the effect of land uplift and sea level rise. The values are averaged

198 over one hour period.

199   Not all the available observations from satellite, moored buoys, CTDs, tide gauges were included

200 in this study. To obtain the high assimilation quality results, another quality control was applied for

201 these data before they were used into assimilation and validation. These controls include examination

202 of forecast observation differences by excluding those observations for which the difference between

203 the forecast and the measurement exceeded given standard maximum deviations. The criteria were set

204 up empirically based on past validation results of the model (Liu et al. 2013). Furthermore, stations

205 located on land, according to the NEMO-Nordic grid, were excluded. We also removed the duplicate

206 records of these data.

207   The accuracy of observation error is difficult to be defined for all water points. The observation

208 is commonly assumed to be spatially irrelevant, which results in an error covariance matrix that is

209 time-invariant diagonal and its diagonal elements equal the variance of observation error. The error for

210 an observation used in data assimilation mainly includes the representation error and the measurement

211 error. The measurement error arises primarily from the measurement device alone, the temporary read-

212 ing error and imperfect retrieval algorithm. According to Janjić et al. (2017), the representation error

213 in data assimilation comprises the error due to unsolved scales or processes, the pre-processing error

214 and the observation-operator error. In this study, the observation error was estimated to one value as

215 the sum of all observation uncertainties used in the analysis. Besides, the uncertainties of satellite SST

216 varies from coast to the open sea, i.e. higher uncertainties in the coast region relative to the open sea.

217 We used a constant standard deviation value of 0.4^{o}C based on the standard deviation of satellite SST,

218 which ranged from the ~0.1^{o}C to ~$0.5\,^{o}$C in the Baltic Sea (She et al. 2007, Høyer et al. 2016).

219

4. Configuration of LSEIK in the experiment

220

221   As above mentioned, the initialization of the filter requires an initial analyzed state and a low

222   rank approximation of the corresponding estimation of error covariance matrix. The data assimilation

223   process was initialized by a free model simulation. First the model was spinning up 20 years to reach a

224   statistically steady state. Then a further (free-run) integration covered the period 2006-2009 was car-

225   ried out to generate a historical sequence of model state. To reduce the calculation cost, we took a

226   snapshot in every 6 days and saved 183 state vectors, which includes sea level, temperature and salini-

227   ty, in total to describe the model variability because successive states are quite similar. The initial en-

228   semble provided an estimate of the initial model state and its uncertainty before the assimilation of

229   SST observations. The quantity of the model variability was expected to be reasonably comparable

230   with the forecast error, which was dominated by misplacement of mesoscale features and varies in

231   location and intensity seasonally. Further, the very high frequencies of model variability were also

232   unfavourable in an ensemble of state vectors for SST data assimilation (Oke et al., 2005). Therefore, a

233   band-pass filter was used to remove the unwanted frequency of model variability. To initial low rank

234   error covariance matrix, a multivariable Empirical Orthogonal Functions (EOF) analysis was applied

235   on the 183 state vectors of model variables (sea level, temperature and salinity). In the North Sea and

236   Baltic Sea, error covariances of different variables are not uniform and strongly dependent on whether

237   the variable resides in the open sea or coastal zone. Each state variable was then normalized by the

238   inverse of its spatially averaged variance at every model level. At last, 34 leading EOF modes were

239   kept and they explained 85% overall variability. Then the initial error covariance matrix was estimated

240   by $P^a(t_0) \approx L_0 U_0 L_0^T$, where the L_0 is composited by the leading EOF modes and U_0 is diagonal

241   matrix with the corresponding eigenvalues on its diagonal. We used a time-invariant sample ensemble

242   to approximate the background error covariance during the experimental period (Korres et al, 2004;

243   Liu et al. 2017). This stationary ensemble affords a good approximation of the ocean's background

244   error covariance. Meanwhile, it is computationally efficient for our objective.

245   The localization scale is another import factor to the assimilation system, especially at the coastal

246 region. Large correlation scale may transfer artificial increments to the positions far away from the

247 analysis observation during the DA process. However, small correlation scale is prone to cause the

248 singularity of ocean state around analyzed observation and break the continuity of the ocean state.

249 Hence, an unreasonable scale causes the instability of the model integration or degrades the assimila-

250 tion quality. Unfortunately, the accuracy length for the correlation is unknown for the North Sea and

251 Baltic Sea. The correlation length scale is to some extent dependent on the Rossby radius of defor-

252 mation (Losa et al., 2012), which varies from ~ 200 km in the barotropic mode to ~ 10 km or even less

253 in the baroclinic mode (Fennel et al., 1991; Alenius et al, 2003). According to the former researches

254 like Liu et al. (2013, 2017), a length scale of 70 km was specified for both the North Sea and Baltic

255 Sea in this study. Not that this value may be not perfect and more accurate correlation length needs to

256 be tested for LSEIK. For example, spatially variable length scales are the next step for the regional DA

257 simulations.

258   To define the forgetting factor, a one-month simulation experiment with varying the factor ρ was

259 done in January 2010. At last, a factor $\rho = 0.3$ resulted in the best assimilation performance. Further,

260 we define a two-day assimilation window in assimilation experiment. As a result, the observations in

261 the two days before the assimilation time were used to calculate the innovation with observation oper-

262 ator. When we calculated the innovation we also changed the observation error according to the obser-

263 vation time by $\varepsilon = 0.4 \times \exp(-0.15\Delta t)$, here Δt is the absolute time difference between observation

264 time and DA time.

265

266 **5. Results**

267   In the following sub-sections, we conducted two runs with and without assimilation of the

268 SST observations from the OSISAF database, both runs with the above setup of the analysis system.

269 Accordingly, the runs with and without assimilation are called ASSIM and FREE, respectively. We

270 considered the evolution of SST based on 48-hourly local analysis from 1 January 2010 to 31 Decem-

271 ber 2010. The 48-hourly forecast SST from two runs was assessed with observations from different

272 dataset. Then we analyzed the impact of the data assimilation on the profile simulation of T/S. At last,

273   we evaluated the system performance with respect to sea surface anormaly and sea ice, respectively.

274

275   **5.1 Comparison with satellite data**

276   First, we presented two cases to show the ocean state before and after the assimilation of the

277   OSISAF SST data in Fig. 2. The first case was given at 11 January 2010, a date with clear weather and

278   many observations available. The model has obvious difficulties in reproducing the observed SST.

279   The cold biases in the forecast were found in the Skagerrak, west coast of the Baltic proper and the

280   Bothnian Bay, respectively. However, the warm biases appeared in the interior of the Baltic Sea and

281   the Kattegat. The largest deviation in the FREE reached 2.2 ^{o}C at the Skagerrak. Apparently, tempera-

282   ture by assimilation analysis agreed with the satellite-derived data much better. This correction at the

283   analysis step has allowed us to reduce the deviation of the SST forecast from the observations. The

284   DA system simulation was also verified at 2 June 2010, which has also many available OSISAF ob-

285   servations. The biases on 2 June 2010 were obviously different from that on 11 January 2010. Moreo-

286   ver, it was found they had a roughly opposite bias signal. For example, relative to the OSISAF SST at

287   the Baltic proper, Bothnian Sea and Bothnian Bay, FREE produced relatively warmer water at January

288   11 and colder water at 2 June (Fig. 2), respectively. After data assimilation, the analysis increments

289   were appropriately added to the model field. In general, the SST DA has improved the simulated SST

290   in both cases (Fig. 2).

291   Maps of annual averaged RMSE of SST from two runs relative to the IceMap observation are

292   shown in Fig. 3. Obviously, the RMSE in FREE and ASSIM had different distribution in the Baltic

293   Sea. In general, FREE had smaller error in the Skagerrak, eastern the Kattegat and the interior of the

294   Bothnian Sea relative to other subbasin of the Baltic Sea. The largest RMSE was found at the connec-

295   tion region between the Baltic proper and the Bothnian Sea. This could be caused by the shallow wa-

296   ter, complicated bathymetry and large observation biases in this area. It was also noted that the RMSE

297   was larger in the coast region compared to its interior in the Baltic proper and Bothnian Sea. After the

298   assimilation, the SST has been significantly improved. The RMSE of SST from ASSIM was generally

299   smaller than 1.0 ^{o}C. However, there were still some regions where the improvements were relatively

300   small and the RMSE of SST was greater than 1.0 ^{o}C. These large errors were predominantly located at

301 the edge of the Baltic Sea and the Danish straits. For instance, the RMSE of SST was greater than 1.2

302 $^{\circ}$C at both the entrance of the Gulf of Finland and the west coast of the Bothnian Sea. The relatively

303 small improvements were regularly caused by the rare observations or the less accurate observations

304 near the coast water.

305   The overall daily averaged SST errors against the IceMap observations have been estimated

306 (Fig. 4). The observations had better coverage in summer and autumn than in winter and spring. The

307 variability of the number of observation directly affected the assessment of DA results. The model

308 biases had pronounced seasonal variability, which had small values in spring and winter. In general,

309 the assimilation provided better SST estimations. The free run had a RMSE of 1.47 $^{\circ}$C. After the as-

310 similation, the RMSE was reduced to 1.03 $^{\circ}$C, whereas the bias was reduced by 0.73 $^{\circ}$C. An interesting

311 feature was that the SST error reduction due to the assimilation was almost consistent with the varia-

312 bility of the number of IceMap observations. For example, the improvement became large with in-

313 creasing the number of IceMap observations from March to June 2010. However, the number of ob-

314 servations was kept constant during the period June-November 2010 and the improvement shown in

315 both the bias and RMSE of SST did not exhibit large variability, which meant reliable performance of

316 the DA system.

317

318 **5.2 Comparison with independent in-situ data**

319   The time series of T/S were compared with independent observations located at Arkona station

320 (13.87°E, 54.88°N) in the Arkona Basin and at BY15 (20.05 $^{\circ}$E, 57.33 $^{\circ}$N) in the Eastern Gotland Ba-

321 sin, respectively. These two stations were selected to verify the experiment results because of their

322 relatively completed observation records for the experiment period. In the Arkona Basin, the water

323 depth was shallow and the water column can be well mixed between surface and bottom water. Thus,

324 the bottom T/S was largely affected by the surface dynamic (Liu et al. 2014). Relative to observations,

325 the model had warm biases at this station (Fig. 5). At a depth of 25m, the observed temperature

326 showed the largest variability, which was a good representation of the bottom characteristics of the

327 mixed layer. In mid-August, the temperature was abruptly increased by 10°C at a depth of 25m and

328 slightly decreased at surface, respectively. The reason is that the surface water suddenly sinks to deep-

329 er layers, which warm the deep water. However, this dynamic process hasn't reached to Arkona bot-

330 tom and it didn't cause the obvious bottom temperature variability (Fig. 9). Both FREE and ASSIM

331 had reproduced this process, whereas FREE showed larger temperature biases. To the salinity at the

332 Arkona station, the surface observations were missing, the comparison at 7 m depth verified the sub-

333 surface simulations. The observations showed larger salinity variability in winter relative to summer.

334 This pronounced seasonal variation is associated with the variation of fresh river runoff and net E–P

335 (Evaporation–Precipitation) flux (Fu et al, 2012). At a depth of 7 m, salinity was obviously underesti-

336 mated from April to September and overestimated after November although the ASSIM had slightly

337 better results compared to FREE. The DA also provided better simulation of salinity at 25 m depth.

338 For example, the salinity bias in the October was reduced by 3 psu by DA. At a depth of 40 m, the

339 saltwater inflows were observed, resulting in sudden increases of salinity. For instance, the salinity

340 was increased by 3.5 psu in February followed by a decreasing trend. The variations were reproduced

341 in both FREE and ASSIM, whereas the intensity of the decreased process is weakly simulated with a

342 difference of 3 psu and the inflow in March was not strong enough relative to the observed one. Ob-

343 servations also showed a large salinity variability amounts to 4–8 psu in the autumn. Although FREE

344 and ASSIM had shown these changes, their magnitude was obvious weaker than observations. The

345 possible reason was that the model's resolution was inadequate to well resolve the topography and

346 eddies in this area. Both the large runoff and the complicated bathymetry posed challenges for the

347 model to tackle the small-scale dynamic process in such a shallow basin. A higher resolution model

348 perhaps was more preferable to study this dynamic process.

349   The Eastern Gotland Basin has deeper water depth compared to the Arkoan Basin, in which the

350 water column is permanently stratified and the halocline lies at about 60–80 m (Fu et al, 2012). The

351 mixing and sinking of T/S are hindered by the strong stratification. Unlike observations in the Arkona

352 Basin (Fig. 5), the CTD observations at BY15 had lower temporal resolution with almost one observa-

353 tion per month. In the mixing layer, it can be seen model had overestimated the temperature (Fig. 6).

354 At a depth of 10 m, ASSIM has remarkably improved the simulation of temperature relative to FREE.

355 The bias has been reduced by 3°C in the spring of 2010. At 175 m depth, observed temperature

356 showed very small variation. The reason was that the main source for deep water ventilation is the

357   saltwater inflows which are suppressed by runoff within a depth range of 75–135 m in the Eastern

358   Gotland Basin (Vali et al. 2013). As a result, updating the bottom water is very slow. Both FREE and

359   ASSIM overestimated the temperature in the spring and the beginning of summer of 2010. Further,

360   ASSIM has increased the temperature bias after mid-summer relative to FREE. This result might be

361   explained by that the strong correlation isn't expected between surface and layers bellow the halocline

362   because of the strong stratification in this basin, which perhaps yield the artificial correction. There-

363   fore, the improvement of the surface temperature cannot guarantee its positive influence on the bottom

364   temperature. To the salinity, the model had less accurate simulation with generally low salinity biases

365   at 10 m depth. ASSIM provided better salinity simulation compared to FREE. At 70 m depth, the

366   small variation of salinity was found after DA. Moreover, at 175 m depth, the observation had very

367   small variability about 0.1 psu. In general, both experiments have reproduced these variations. How-

368   ever, FREE increased salinity by 0.2 psu from March to April relative to the observation, which

369   caused the overall salinity overestimated amount to 0.2 psu. This increasing process wasn't shown in

370   observations and the reason remained unclear. The DA has shown slight improvement, but it still salt-

371   er than the observations.

372   The mixed layer depth (MLD) was calculated at the Arkona and BY15 station and compared with

373   the SHARK observation in Fig. 7. We used the temperature criterion to define the MLD, i.e., the depth

374   at which the temperature deviated from the surface value by 0.5 ^{o}C (Fu et al., 2012). Figure 7 shows

375   that the MLD at Arkona had larger variability relative to the MLD at BY15. The reason contributed to

376   this feature is that the deeper water at Arkona is easy affected by wind forcing because of the shallow

377   bathymetry and well mixing, whereas the temperature variation in upper water at BY15 difficulty in-

378   fluences the deeper water because of the strong stratification. Both runs had reproduced the MLD var-

379   iability feature similar as the observations. For example, the minimum MLD appeared in summer,

380   which was about several meters. The assimilation of satellite SST caused strong changes in the MLD

381   at both stations, especially in winter. One explanation was that the Baltic Sea was largely affected by

382   wind forcing and the winter wind was much stronger than the summer wind. Further, strong heating in

383   summer promoted stratification in summer and shoaled the MLD.

384   Further, the temporal and spatial distribution of the SHARK observations is shown in Fig.8.

385   These observations were unevenly distributed in the Baltic Sea. In the Skagerrak, the observations

386   appeared at the Danish and Swedish coast. However, in the Bornholmn Basin, Kattegat, and Baltic

387   proper, the observations mainly were found in the central and the Swedish coast side. There were also

388   many observations in the Bothnian Sea and rare observations in the central of the Bothnian Bay. It

389   must be noticed that there aren't SHARK observations in both the Gulf of Finland and Gulf of Riga

390   during the experiment period. Moreover, these SHARK profiles in the first four months were mainly

391   located from the Skagerrak to the Baltic proper, which are relatively rare in the northern Baltic Sea. In

392   the Bothnian Bay, the observations are mainly in the winter period.

393   Figure 9 shows the change of overall bias and RMSE of T/S with depth against the SHARK

394   dataset. In the Baltic Sea, DA had large impact on the temperature forecast in the water above 100 m.

395   The RMSE showed that the forecast of temperature was obviously improved from surface to thermo-

396   cline in the ASSIM and the improvements generally decreased with depth. Above 100 m, the overall

397   RMSE of temperature in ASSIM was decreased by 21.38% (from 1.59 to 1.25 $^{\circ}$C). It was also found

398   the temperature error had similar variability as the warm biases in two runs. In the transition zone, the

399   RMSE in the ASSIM was reduced by 5.59% and -20.31% above and below 100 m relative to the

400   FREE, respectively. Below 90 m, the temperature was also over-adjusted, which changed the warm

401   bias to cold bias. It is worth noting that the number of the deeper water observation in the transition

402   zone is substantially less than that in the Baltic Sea. For the salinity, both RMSE and bias of the AS-

403   SIM showed very minor changes relative to the FREE inside the Baltic Sea. For the water above 100

404   m, the total RMSE of salinity was increased by 3.48% (from 1.15 psu in the FREE to 1.19 psu in the

405   ASSIM) in the transition zone and 1.04% (from 0.96 psu in the FREE to 0.97 psu in the ASSIM) in

406   the Baltic Sea.

407

408   **5.3 Sea Level Anomaly**

409   SLA represents a vertically integrated effect of the T/S variations over the whole water col-

410   umn. The accurate simulation of SLA is thus a good indicator of the model performance. Therefore,

411   validating the impact of SST assimilation on the simulation of SLA is very important to the Baltic Sea

412   forecast. The observations from the 24 tide gauge stations were used. These gauge stations are mainly

413   located at the Swedish coast (see Fig.8b). Since only the SST is assimilated in this study, the SLA

414   observations are completely independent.

415   We calculated the RMSE and correlation coefficients for both the FREE and ASSIM against the

416   observations from tide gauges (Fig. 10). The overall RMSE was reduced by 1.8% and the correlation

417   coefficients were slightly increased. Among these stations, RMSE at the Oskarshamn was decreased

418   by 5.6%, which is larger than that in other station. The minimum RMSE change of SLA was seen at

419   the Klagshamn. For the correlation coefficient, improvement on the SLA by the DA is very small.

420   Simrishamn station showed the biggest change of correlation coefficient, which is 1.1%. The RMSE

421   and correlation comparison demonstrated that the SST DA has generally positive effects on the fore-

422   cast of the SLA.

423   In addition, the time series of the SLA error discrepancy (ASSIM minus FREE) in two runs at

424   four stations were selected to evaluate the simulation results (Fig. 11). These four stations were select-

425   ed to represent the model performance at different positions of the Swedish coast. Two runs showed

426   evidently different performance in these four stations. The variability of the SLA difference between

427   two experiments at the Smogen station had higher frequency compared to other stations. The reason

428   was that the Smogen station was located at the transition zone where the water had higher frequency

429   variations caused by the brackish Baltic in/outflowing relative to other three stations. At these four

430   stations, the improvements were mainly in later spring and summer, whilst the degraded simulations

431   were mostly happened after Mid-September, respectively. The SST assimilation had less impact in late

432   winter and early spring compared to other seasons. Besides, the impact of SST assimilation on SLA

433   simulation was not same in the four positions. For instance, during the period from Mid-November to

434   Mid-December, the SLA in ASSIM was improved at Simrishamn and degraded at both the Ratan and

435   LandsortNorra stations, respectively. This phenomenon was possibly caused by the imperfect correla-

436   tion between SST and SLA in the stationary samples. Further, these steric small changes of SLA by

437   DA were what we expected because only SST was assimilated into Nemo-Nordic.

438

439   **5.4 Sea ice**

440   Sea ice in the Baltic Sea occurs primarily in its north region and influences the Baltic climate.

441 Accurate detecting the sea ice is very useful to the northern Baltic living because too much or too little

442 sea ice can be a problem for wildlife and people. Sea ice concentration (SIC) and Sea ice extent (SIE)

443 are two important and common indicator to modeling sea ice environment. We assessed the SIC and

444 SIE from simulations against the IceMap observations in Fig. 12-13. Differ from the daily evaluation

445 in Losa et al. (2014), the monthly mean SIC was used to represent the general status of sea ice in the

446 Baltic Sea. Besides, SIC in January, February and December showed the variation of the sea ice in

447 winter.

448  In January 2010, the observations showed large ice coverage in the Bothnian Bay and the Gulf

449 of Finland and small SIC in the Gulf of Riga, respectively. Model generally reproduced this distribu-

450 tion of sea ice. However, FREE simulated too much sea ice in the Gulf of Finland and the eastern

451 coast of the Baltic proper relative to observations. For example, SIC from FREE almost to 30% higher

452 than observations along the Estonia coastline. It could be seen that the SST DA reduced these biases.

453 The reason is the SST DA modified the thermal expansion by providing the well temperature fields

454 above the thermocline. The temperature in February became colder relative to January in the Baltic

455 Sea. As a result, the sea ice in February extended to the Bothnian Sea and the whole Gulf of Riga.

456 Observation also showed small SIC in Kattegat and Skagerrak. Model simulated higher SIC in the

457 Bothnian Sea with largest biases along the Swedish and Finnish coast. As an example, the observed

458 ice in the Bothnian Sea was characterized by concentrations mainly smaller than 0.5, whereas modeled

459 ice in FREE had concentration greater than 0.9 in the shallow region of the Bothnian Sea. FREE also

460 had smaller ice coverage with lower SIC in the transition zone between the North Sea and the Baltic

461 Sea relative to IceMap. After the SST assimilation, ASSIM reduced SIC in the Bothnian Bay and the

462 west coast of the Baltic Sea, which was closer to the observations. The ice in ASSIM didn't have ob-

463 vious variation in Kattegat and Skagerrak yet. ASSIM also reduced too much ice at the southern of the

464 Bothhomn Basin. The reason is that the satellite SST observations had limited accuracy near the coast

465 and they could bring artificial information into the modeling. In March, compared to observation, the

466 FREE produced low SIC in the western coast of the Bothnian Sea, Gulf of Finland, Gulf of Riga and

467 the connect zone between the Bothnian Sea and Gulf of Finland. However, the model SIC in the FREE

468 was higher than IceMap in the interior the Bothnian Bay. For instance, the SIC from FREE in the

western Bothnian Sea was 40% higher than observation. In the south coast of the Arkona basin and Baltic proper, the FREE failed to reproduce the sea ice as in observation. After the DA, the high SIC was decreased in western Bothnian Sea and closer to that in IceMap in Bothnian Sea. In the Gulf of Finland and Gulf of Riga, the SIC error was increased in the ASSIM. In April, the large SIC error in the FREE was shown in the Bothnian Sea, the Bothnian Bay, Gulf of Rig and Gulf of Finland, where no clear improvements were seen in the ASSIM. In December, sea ice coverage was smaller because of relatively warm temperature compared to that in other winter month. Most of the sea ice with high concentration was observed at the edge of the Bothnian bay. Nevertheless, high concentration ice in FREE also happened at the transition zone between the Bothnian Sea and Bothnian bay. Relatively, ASSIM reduced the high concentration biases of sea ice. By contrast, both ASSIM and FREE had lower concentration ice than observation in the eastern coast of the Bothnian Sea. The SIC from AS-SIM was relatively lower than that from FREE in the northern Finish coast, whereas the observations had high concentration ice there.

The daily SIE from FREE and ASSIM was compared with observations in Fig.13. The observed SIE was generally increased from January to February and reached the maximum in mid-February. During the period of March-May, SIE was decreased as temperature was increasing. SIEs in both the FREE and ASSIM experiments were generally underestimated by comparison with the observation in 2010, especially in the period from Mid-March to early April. The SIE bias in both runs was roughly increased from January to early April. In early April, the maximum negative bias of SIE was found to be 105000 km^2 for ASSIM and 10000 km^2 for FREE. The impact of SST assimilation on the SIE was positive during the phase of sea ice formation. For example, the SIE bias was reduced 25000 km^2 at end of February and in the Mid-December. However, during the phase of sea ice melting (March to April), the SIE error was increased in ASSIM even with the error of SST decreased. For example, the SIE bias in ASSIM was increased by 42000 km^2 relative to FREE in the early March. These increased SIE error in March mainly happened in the Gulf of Riga and Gulf of Finland (Fig.11).

6. Conclusion and discussions

496   A DA system based on a LSEIK filter has been coupled to the NEMO circulation model of the

497   North and Baltic Seas. The method was successfully applied for assimilating high resolution satellite

498   SST data. We demonstrated that, over the period of 2010, the agreement of the SST forecast with the

499   independent satellite observation was improved by ~ 29.93% in comparison with the regular forecast

500   without DA. The assimilation quality is directly related to the number of observation.

501   Compared with independent in-situ data from SHARK, the RMSE of temperature was reduced

502   by 21.38% and 5.59% for the water above 100 m inside and outside of the Baltic Sea, respectively.

503   However, in the deeper layers, the temperature was slightly degraded in the Baltic Sea. This is partial-

504   ly caused by the artificial correlation between surface layer and deeper layers. The improvement of

505   temperature by SST DA can't guarantee corresponding improvement of the salinity. The statistics

506   displays the salinity RMSE was increased by 1.04% and 3.48% in the transition zone and the Baltic

507   Sea, respectively. Both ASSIM and FREE have captured the main dynamic process in the Baltic Sea,

508   for example, the inflow and the sink. However, ASSIM is closer to the observed one relative to

509   FREE.

510   The forecast results were further validated with the independent SLA observations. The result

511   shows that all RMSEs and correlations for all 21 stations are smaller than 0.12 m and greater than

512   0.86, respectively. After DA, the SLAs at these stations have been slightly improved. In general, the

513   RMSE was reduced by 1.8% and correlation coefficients were slightly increased, respectively. Fur-

514   ther, the model-observation comparison at selected four stations indicates that these improvements are

515   mainly in later of spring and summer. The comparisons also denote the SST assimilation has less im-

516   pact in the late winter and early spring relative to other seasons.

517   When compared with monthly mean observations of SIC, both assimilation run and free run

518   reproduced main spatial distributions of sea ice in the Baltic Sea. During the sea ice formation period,

519   the SST assimilation has improved the results of SIC from FREE in the Gulf of Finland, the Bothnian

520   Sea and eastern coast of the Baltic proper. However, minor improvements were found in Kattegat and

521   Skagerrak. Besides, over the sea ice melting period, the SIE comparison showed the SST assimilation

522   increased the SIE error, especially in the Gulf of Finland and Gulf of Riga.

523   The daily MLD from two runs has been compared with the observations at Arkona and BY15

524   stations. Model could capture the variability features of the MLD. Similar as Fu et al.(2012), it was

525   found that SST assimilation had less impact on the MLD in summer than that in winter. In general, the

526   SST DA produced less influences on the MLD in the deeper region (BY15) relative to that in the shal-

527   low region (Arkona).

528   Further, the reliability of the DA system is worth being assessed. In Rodwell et al.(2006), a per-

529   fect reliable system error variance for ensemble assimilation was calculated by the sum of the variance

530   of the sample ensemble, the square of innovation(misfit between observation and model) and the vari-

531   ance of observation at assimilation time. In this study, we used a constant observation error similar to

532   Rodwell et al. (2016) because our DA design is different from that paper. The major difference be-

533   tween these two studies is that we estimate the background error covariance from stationary ensemble

534   and avoid the perturbation of observation error. Therefore, the variance of the sample ensemble and

535   observation is univariate and the diagnostic of the assimilation stability can be directly obtained from

536   the forecast error like the RMSE in Fig.4.

537   The results of the SST assimilation are encouraging and the assimilation helps to ameliorate

538   some model deficiencies such as the simulation of sea ice in the Gulf of Finland. However, some prob-

539   lems need to be further addressed in the SST DA in the future: firstly, the SST assimilation has worse

540   influence on the simulation of salinity in the upper layers and temperature in the deeper layers. Losa et

541   al.(2012) denoted that the salinity simulation quality crucially depends on the assumptions about the

542   model and data error statistics. Here a stationary ensemble sample was used to represent the correla-

543   tion between T/S and between surface and deep water. These relationships could be changed with the

544   varying dynamics and forcing conditions. More sophisticated assumption should be used in the DA of

545   Baltic Sea. Secondly, the SHARK observations in this study are absent at the Gulf of Finland and Gulf

546   of Riga. This denotes the validation results with SHARK observation didn't include the evaluation of

547   the simulation of T/S in deep water of these two basins. Thirdly, the univariate localization scale used

548   in this study could be another problem. The spreading of observation information strongly depended

549   on the correlation scale. The large localization scale can introduce the artificial information, which

550   could degrade the assimilation quality. A flow-dependent background error covariance with varying

551   correlation scale may be more appropriate for the Baltic Sea with complex bathymetry and rich dy-

552 namics. Fourthly, the remote sensing observations near the coast could have large bias because of the

553 limit of the instrument itself. More strict quality controlling method needed to be used for the satellite

554 coastal observations before their assimilation.

555

556 Appendix

557 Here, we describe the details of the mathematical formulation used in the forecast and correction

558 (analysis) steps of the LSEIK filter:

559 1. Forecast: the analysis state $\mathbf{X}^a$ at time t_{i-1} is integrated forward to the time of the next available

560 observations t_i to compute the forecast state $\mathbf{X}^f$,

561 $$\mathbf{X}^f(t_i) = \mathbf{M}(t_{i-1}, t_i)\mathbf{X}^a(t_{i-1}) \qquad (1),$$

562 where $\mathbf{M}$ denotes the nonlinear dynamic model operator that integrates a model state from time t_{i-1}

563 to time t_i. The superscript $'f'$ and $'a'$ denote the forecast and analysis. The corresponding error covar-

564 iance matrix can be expressed as:

565 $$\mathbf{P}^f(t_i) = \mathbf{L}_i[(r+1)\mathbf{T}^T\mathbf{T}]^{-1}\mathbf{L}_i^T + \mathbf{Q}_i \qquad (2),$$

566 $$\mathbf{L}_i = \mathbf{X}^f(t_i)\mathbf{T} \qquad (3),$$

567 with $\mathbf{Q}_i$ being the covariance matrix of model uncertainties and $r+1$ is the minimum number of

568 sample ensemble members for error covariance matrix. The superscript $'T'$ denotes the transpose of

569 matrix. The full rank matrix $\mathbf{T}$ has a dimension of $(r+1) \times r$ with zero column sums and $\mathbf{L}$ is a full

570 rank $(r+1) \times r$ matrix which implicitly represents the model variability.

571 2. Correction: when the observation is available at time t_i, the LSEIK filter merged the information

572 from model and observation to produce the analysis state with the formula:

573 $$\mathbf{X}^a(t_i) = \mathbf{X}^f(t_i) + \mathbf{K}_i[\mathbf{Y}^o(t_i) - \mathbf{H}_i\mathbf{X}^f(t_i)] \qquad (4).$$

574 Here $\mathbf{Y}^o$ is a vector of observations. The gain matrix $\mathbf{K}$, which linearly interpolates between the obser-

575 vations and the forecast, is given by

576 $$\mathbf{K}_i = \mathbf{P}_i^f\mathbf{H}_i^T\left(\mathbf{H}_i\mathbf{P}_i^f\mathbf{H}_i^T + \mathbf{R}_i\right)^{-1} = \mathbf{L}_i\mathbf{U}_i(\mathbf{H}_i\mathbf{L}_i)^T\mathbf{R}_i^{-1} \qquad (5),$$

577 where $\mathbf{H}_i$ denotes the linearization of observation operator, which mapping the model space to the

578   observation space. $\mathbf{R}$ is the observation error covariance matrix. The matrix $\mathbf{U}_i$ is updated according to

579
$$\mathbf{U}_i^{-1} = \rho(r+1)\mathbf{T}^T\mathbf{T} + \mathbf{L}_i^T\mathbf{H}_i^T\mathbf{R}_i^{-1}\mathbf{H}_i\mathbf{L}_i \qquad (6).$$

580   Here ρ is A forgetting factor.

581   A second-order exact sampling is used to initialize the LSEIK filter. At time t_{i-1}, a analysis

582   state $\mathbf{X}^a(t_{i-1})$ and its corresponding error covariance matrix $\mathbf{P}^a(t_{i-1})$, in the factorized form

583    $\mathbf{L}_{i-1}\mathbf{U}_{i-1}\mathbf{L}_{i-1}^T$, are available. The samples can be given by the following formular:

584
$$\mathbf{X}_k^a(t_{i-1}) = \overline{\mathbf{X}^a}(t_{i-1}) + \sqrt{r+1}\mathbf{L}_{i-1}\left(\mathbf{\Omega}_{k,i-1}\mathbf{C}_{i-1}\right)^T \qquad (7).$$

585   For $1 \leq k \leq r+1$, the $\mathbf{C}_{i-1}$ is the Cholesky decomposition of $\mathbf{U}_{i-1}^{-1}$ and Ω_{i-1} is a $(r+1) \times r$ ma-

586   trix with orthonormal columns and zero column sums, where $\mathbf{\Omega}_{k,i-1}$ denotes the kth row of $\mathbf{\Omega}_{i-1}$. $\overline{\mathbf{X}^a}$

587   is the average of the analysis state.

588

589   **Acknowledgment**

590   The research presented in this study was funded by the Swedish Space Board within the project 'As-

591   similating SLA and SST in an operational ocean forecasting mode for the North Sea and Baltic Sea

592   using satellite observations and different methodologies' (grant no.172/13). We thank Dr. Svetlana

593   Losa and one anonymous reviewer for their valuable comments that helped improve the manuscript.

594

595   **References**

596   Adcroft, A., and Campin, J. M.: Re-scaled height coordinates for accurate representation of free-

597   surface flows in ocean circulation model, Ocean Modell., 7, 269–284, 2004.

598

599   Alenius, P. A., Nekrasov, A., and Myrberg, K.: Variability of the baroclinic Rossby radius in the Gulf

600   of Finland, Cont. Shelf Res., 23 (6), 563–573, 2003.

601

602   Beckmann, A., and Döscher, R.: A method for improved representation of dense water spreading over

603   topography in geopotential-coordinate models, J. Phys. Oceanogr., 27, 581–591, 1997.

604

605 Brisson, A., Le Borgne, P., and Marsouin, A.: Results of one year of preoperational production of sea

606 surface temperatures from GOES-8, J. Atmos. Oceanic Technol., 19(10), 1638–1652, 2002.

607

608 Dahlgren, P., Kållberg, P., Landelius, T. and Undén, P.,: EURO4M Project Report, D 2.9 Comparison

609 of the Regional Reanalyses Products with Newly Developed and Existing State-of-the Art Systems.

610 Technical Report, Online at: http://www.euro4m.eu/Deliverables.htm, 2014.

611

612 Donnelly, C., Andersson, J. C., and Arheimer, B.: Using flow signatures and catchment similarities to

613 evaluate the E-HYPE multi-basin model across Europe, Hydrological Sciences Journal, 61, 255–273,

614 2016.

615

616 Egbert, G. D., and Erofeeva, S. Y.: Efficient inverse modeling of barotropic ocean tides, J. Atmos.

617 Oceanic Technol., 19(2), 183–204, doi: 10.1175/1520-0426, 2002.

618

619 Fennel, W., Seifert, T., and Kayser, B.: Rossby radii and phase speeds in the Baltic Sea. Cont. Shelf

620 Res., 11(1), 23–26, 1991.

621

622 Fu, W.W., She, J., and Dobrynin, M.: A 20-year reanalysis experiment in the Baltic Sea using

623 three-dimensional variational (3DVAR) method. Ocean Sci., 8, 827–844, 2012.

624

625 Galperin, B., Kantha, L. H., Hassid, S., and Rosati A.: A quasi-equilibrium turbulent energy model for

626 geophysical flows, J. Atmos. Sci., 45, 55–62, 1988.

627

628 Haines, K.: Ocean data assimilation. In: Data Assimilation: Making Sense of Observations. . Springer-

629 Verlag, Berlin Heidelberg, pp. 517-548. ISBN 9783540747024, 2010.

630

631 Hordoir, R., Axell, L., Löptien, U., Dietze, H., and Kuznetsov, I.: Influence of sea level rise on the

632   dynamics of salt inflows in the Baltic Sea, J. Geophys. Res. Oceans, 120, doi:10.1002/2014JC010642,

633   2015.

634

635   Hordoir, R., Dieterich, C., Basu, C., Dietze, H., and Meier M.: Freshwater outflow of the Baltic Sea

636   and transport in the Norwegian current: A statistical correlation analysis based on a numerical experi-

637   ment, Cont. Shelf Res., 64, 1–9, doi:10.1016/j.csr.2013.05.006, 2013.

638

639   Høyer J.L., and Karagali, I.: Sea Surface Temperature Climate Data Record for the North Sea and

640   Baltic Sea. JOURNAL OF CLIMATE. 29, 2529–2541, 2016.

641

642   Janjić, T., Nerger, L., Albertella, A., Schröter, J., Skachko, S.: On domain localization in ensemble

643   based Kalman filter algorithms. Monthly Weather Review, 136 (7), 2046–2060, 2011.

644

645   Janjić, T. , Bormann, N. , Bocquet, M. , Carton, J. A., Cohn, S. E., Dance, S. L., Losa, S. N., Nichols,

646   N. K., Potthast, R. , Waller, J. A. and Weston, P.: On the representation error in data assimilation.

647   Q.J.R. Meteorol. Soc.. doi:10.1002/qj.3130, 2017.

648

649   Kilpatrick, K. A., Podesta, G. P., and Evans, R.: Overview of the NOAA/NASA Advanced Very High

650   Resolution Radiometer Pathfinder algorithm for sea surface temperature and associated matchup data-

651   base, J. Geophys. Res., 106(C5), 9179–9197, doi:10.1029/1999JC000065, 2001.

652

653   Large, W. G., and Yeager, S.: Diurnal to decadal global forcing for ocean and sea-ice models: The

654   data sets and flux climatologies, NCAR Tech. Note, NCAR/TN-4601STR, CGD Div. of the Natl.

655   Cent. for Atmos. Res., 2004.

656

657   Leclair, M., and Madec, G.: A conservative leapfrog time stepping method, Ocean Modell., 30, 88–94,

658   doi:10.1016/j.ocemod.2009.06.006, 2009.

659

660   Leppäranta, M., and Myrberg, K.: The Physical Oceanography of the Baltic Sea, pp. 378, Springer-

661   Verlag, Berlin-Heidelberg, New York, 2009.

662

663   Levitus, S., and Boyer, T. P.: Salinity, in World Ocean Atlas 1994, NOAA Atlas NESDIS, vol. 3, 99

664   pp., U.S. Gov. Print. Off., Washington, D. C., 1994.

665

666   Liu, Y., Zhu, J., She, J., Zhuang, S. Y., Fu, W.W., and Gao, J.D.: Assimilating temperature and salini-

667   ty profile observations using an anisotropic recursive filter in a coastal ocean model. Ocean Model. 30,

668   75–87, 2009.

669

670   Liu, Y., Meier, H. E. M., and Axell, L.: Reanalyzing temperature and salinity on decadal time scales

671   using the ensemble optimal interpolation data assimilation method and a 3-D ocean circulation model

672   of the Baltic Sea. J. Geophys. Res.Oceans., 118, 5536–5554, 2013.

673

674   Liu, Y., Meier, H. E. M., and Eilola, K.: Improving the multiannual, high-resolution modelling of bio-

675   geochemical cycles in the Baltic Sea by using data assimilation, Tellus A, 66, 24908,

676   doi:10.3402/tellusa.v66.24908, 2014.

677   Liu, Y., Meier, H. E. M., and Eilola, K.: Nutrient transports in the Baltic Sea – results from a 30-year

678   physical–biogeochemical reanalysis. Biogeosciences, 14, 2113–2131, 2017.

679

680   Losa S.N., Danilov, S., Schröter, J., Nerger, L., Maβmann, S., and Janssen, F.: Assimilating NOAA

681   SST data into the BSH operational circulation model for the North and Baltic Seas: Inference about

682   the data. Journal of Marine Systems, 105–108,152–162, 2012.

683

684   Losa S.N., Danilov, S., Schröter, J., Janjic, J., Nerger, L., and Janssen, F.: Assimilating NOAA SST

685   data into the BSH operational circulation model for the North and Baltic Seas: Part 2. Sensitivity of

686   the forecast's skill to the prior model error statistics. Journal of Marine Systems, 259–270, 2014.

687

688 Madec, G.: NEMO ocean engine, version 3.3, Note du Pôole de modélisation de l'Inst. Pierre-Simon

689 Laplace 27, Inst. Pierre-Simon Laplace, Paris. (Available at http://www.nemo-ocean.eu/.), 2010.

690

691 Malanotte-Rizzoli, P, and Tziperman, E.: The oceanographic data assimilation problem: overview,

692 motivation and purposes. In Modern Approaches to Data Assimilation in Ocean Modeling, Amster-

693 dam: Elsevier, 3–17, 1996.

694

695 Nerger, L., Danilov, S., Hiller, W., and Schröter, J.: Using sea level data to constrain a finite-element

696 primitive-equation ocean model with a local SEIK filter. Ocean Dynamics 56, 634–649, 2006.

697

698 Nowicki, A., Dzierzbicka-Głowacka, L., Janecki, M., and Kałas, M.: Assimilation of the satellite SST

699 data in the 3D CEMBS model. Oceanologia, 57, 17–24, 2015.

700

701 O'Dea E. J., Arnold, A. K., Edwards, K. P., Furner, R., Hyder, P., Martin, M. J., Siddorn, J. R.,

702 Storkey, D., While, J., Holt, J. T., and Liu H.: An operational ocean forecast system incorporating

703 NEMO and SST data assimilation for the tidally driven European North-West shelf, Journal of Opera-

704 tional oceanography, 5(1), 3-17, 2012.

705

706 Oke, P. R., Schiller, A., Griffin, D. A., and Brassington, G. B.: Ensemble data assimilation for an ed-

707 dy-resolving ocean model of the Australian Region. Q. J. Roy. Meteorol. Soc. 131, 3301–3311, 2005.

708

709 Omstedt, A., Elken, J., Lehmann,A., Leppäranta, M., Meier, H.E.M., Myrberg, K., and Rutgersson,

710 A.: Progress in physical oceanography of the Baltic Sea during the 2003–2014 period. Progress in

711 Oceanography, 128, 139-171, 2014.

712

713 Pham, D.T.: Stochastic methods for sequential data assimilation in strongly nonlinear systems. Mon.

714 Weather Rev. 129, 1194–1207, 2001.

715

716   Pham, D. T., Verron, J. and M. C. Roubaud: A singular evolutive extended Kalman filter for data as-

717   similation in oceanography. J. Mar. Syst.,16, 323–340, 1998.

718

719   Rodwell, M. J., Lang, S. T. K., Ingleby, N. B., Bormann, N., Hólm, E., Rabier, F., Richard-

720   son, D. S., and Yamaguchi, M.: Reliability in ensemble data assimilation, Q. J. Roy. Meteor. Soc.,

721   142, 443–454, doi:10.1002/qj.2663, 2016.

722

723   Samuelsson, P., Jones, C., Willen, U., Ullerstig, A., and co-authors.: The Rossby Centre Regional

724   Climate model RCAS3: model description and performance, TellusA, 63, 4–23, 2011.

725

726   She, J, Høyer, J. L., and Larsen, J.: Assessment of sea surface temperature observational networks in

727   the Baltic Sea and North Sea. Journal of Marine Systems 65, 314–335, 2007.

728

729   Stramska, M., and Białogrodzka, J.: Spatial and temporal variability of sea surface temperature in the

730   Baltic Sea based on 32-years (1982—2013) of satellite data. Oceanologia, 57, 223–235, 2015.

731

732   Tranchant B., Reffray, G., Greiner, E., Nugroho, D., Koch-Larrouy, A., and Gaspar, P.: Evaluation of

733   an operational ocean model configuration at $1/12\circ$ spatial resolution for the Indonesian seas

734   (NEMO2.3/INDO12) –Part 1: Ocean physics. Geosci. Model Dev., 9, 1037–1064, 2016.

735

736   Umlauf, L., and Burchard, H.: A generic length-scale equation for geophysical turbulence models, J.

737   Mar. Syst., 61, 235–265, 2003.

738

739   Vancoppenolle, M., Fichefet, T., Goosse, H., Bouillon, S., Madec, G., and Maqueda, M. A. M.: Simu-

740   lating the mass balance and salinity of arctic and Antarctic sea ice, Ocean Modell., 27(1–2), 33–53,

741   doi:10.1016/j.ocemod.2008.10.005, 2008.

742

743   Väli, G., Meier, H. E. M., and Elken, J.: Simulated halocline variability in the Baltic Sea and its im-

744 pact on hypoxia during 1961–2007, J. Geophys. Res.-Ocean., 118, 6982–7000,

745 doi:10.1002/2013JC009192, 2013.

746

747 Walton, C. C., Pichel, W. G., Sapper, F. J., and May, D. A.: The development and operational applica-

748 tion of nonlinear algorithms for the measurement of sea surface temperatures with NOAA polar-

749 orbiting environmental satellites, J. Geophys. Res., 103(C12), 27,999–28,012,

750 doi:10.1029/98JC02370, 1998.

751

752

753

754

755

756

757

758

759

760

761

762

763

764

765

766

767

768

769

770

771

772   Figure 1. Geographical domain and bathymetry (in m) of the NEMO-Nordic configuration.
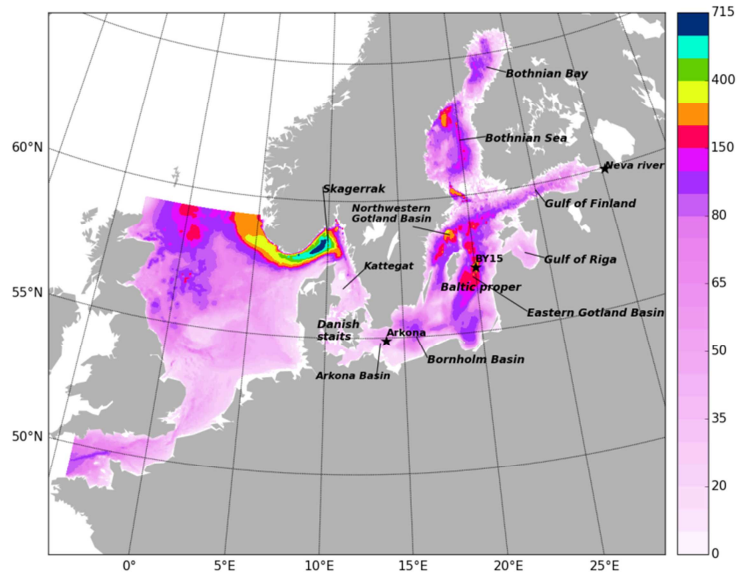
773

774

775

776

777

778

779

780

781

782

783

784

785

786

787
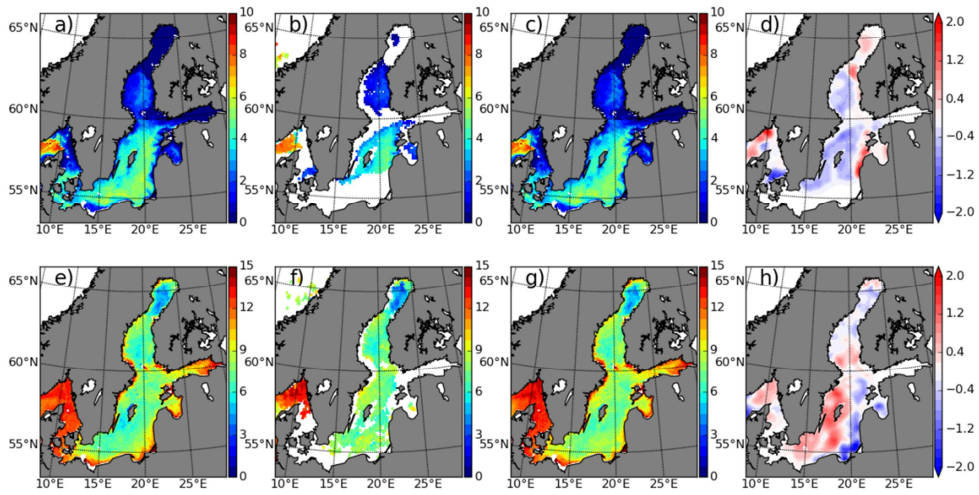
788

789   Figure 2. Map of SST from FREE (a,e), OSISAF (b, f), ASSIM (c, g) and the assimilation increments

790   (d, h) on 11 January 2010 (first row) and 2 June 2010 (second row), respectively.

791

792

793

794

795

796

797

798

799

800

801

802

803

804

805
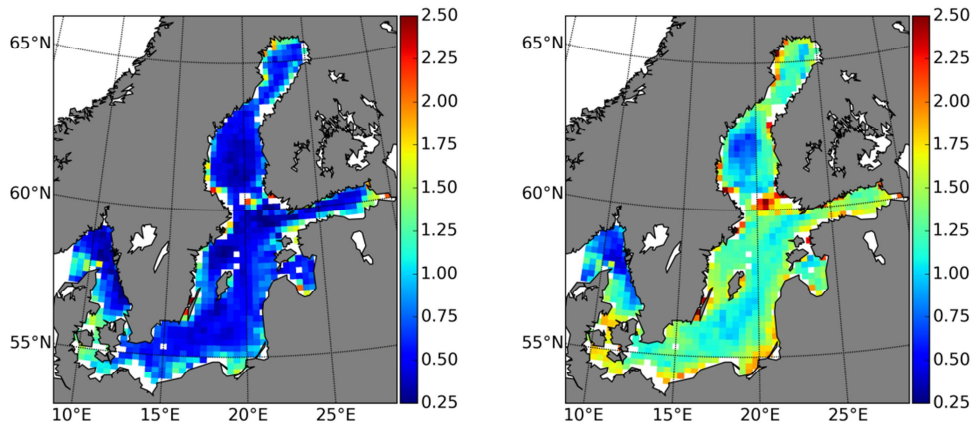
806

807 Figure 3. Map of the RMSE of SST from ASSIM (left panel) and FREE (right panel) calculated

808 against IceMap SST in 2010, respectively.

809

810

811

812

813

814

815

816

817

818

819

820

821

822

823

824

825

826
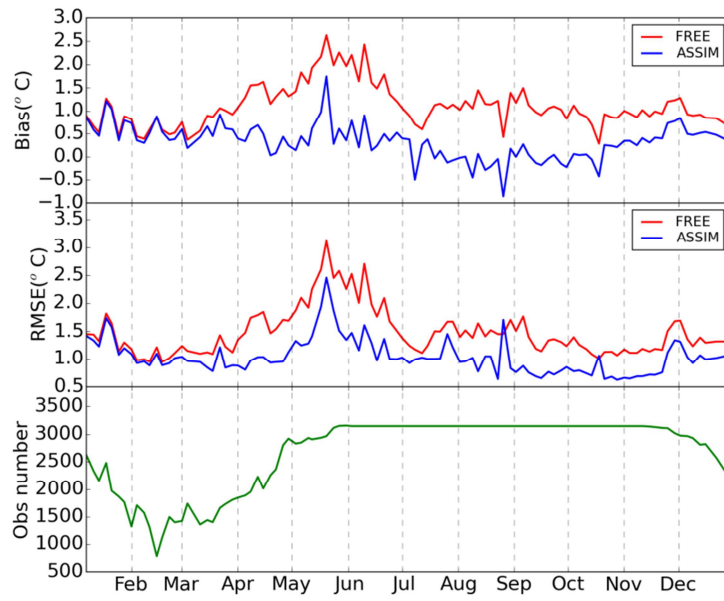
827

828   Figure 4. The evolution of basin-averaged bias and RMSE of SST from FREE and ASSIM relative to

829   IceMap SST and the number of IceMap observation in 2010.

830

831

832

833

834

835

836

837

838

839

840

841

842
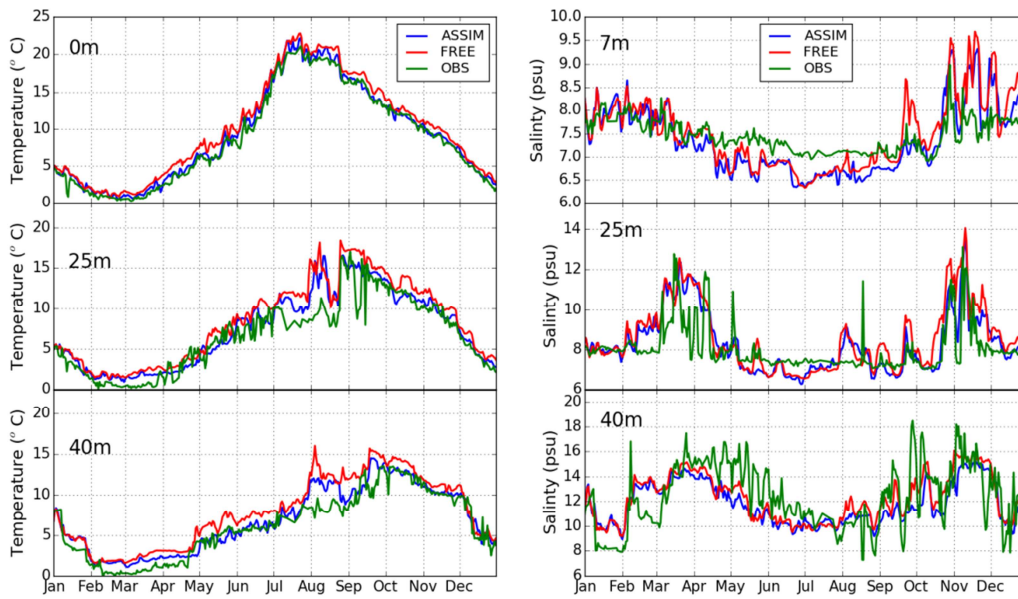
843

844   Figure 5. The time series of temperature (left panel) at a depth of 0, 25 and 40 m and salinity (right

845   panel) at a depth of 7, 25 and 40 m at the Arkona station (13.87^{o}E, 54.88^{o}N), respectively.

846

847

848

849

850

851

852

853

854

855

856

857

858

859
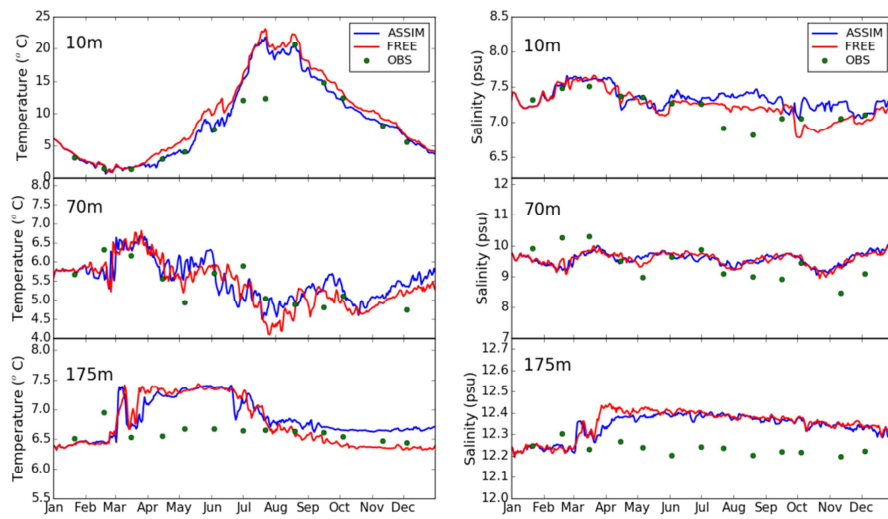
860

861   Figure 6. The time series of temperature (left panel) and salinity (right panel) at the BY15 station

862   (20.05°E, 57.33°N) at a depth of 10, 70 and 175 m, respectively.

863

864

865

866

867

868

869

870

871

872
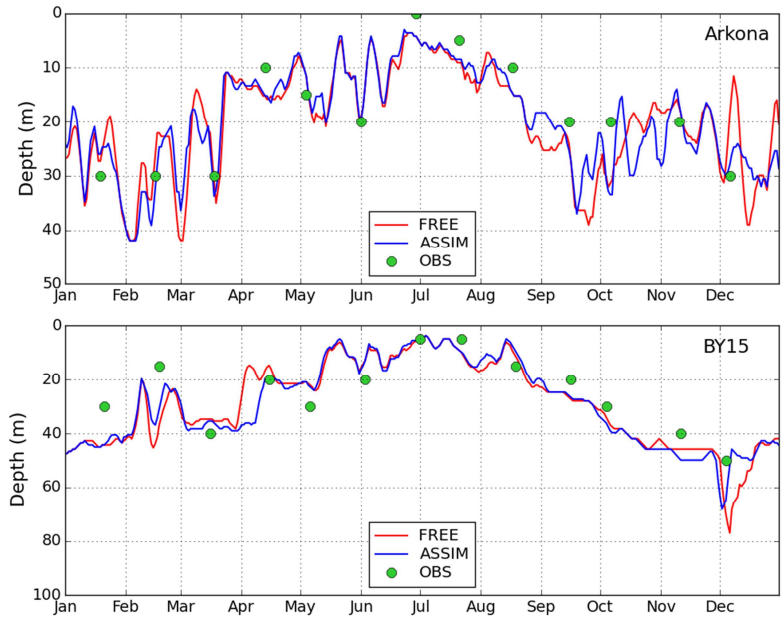
873

874 Figure 7. The time series of mixed layer depth at Arkona and BY15 station.

875

876

877

878

879

880

881

882

883

884

885

886

887
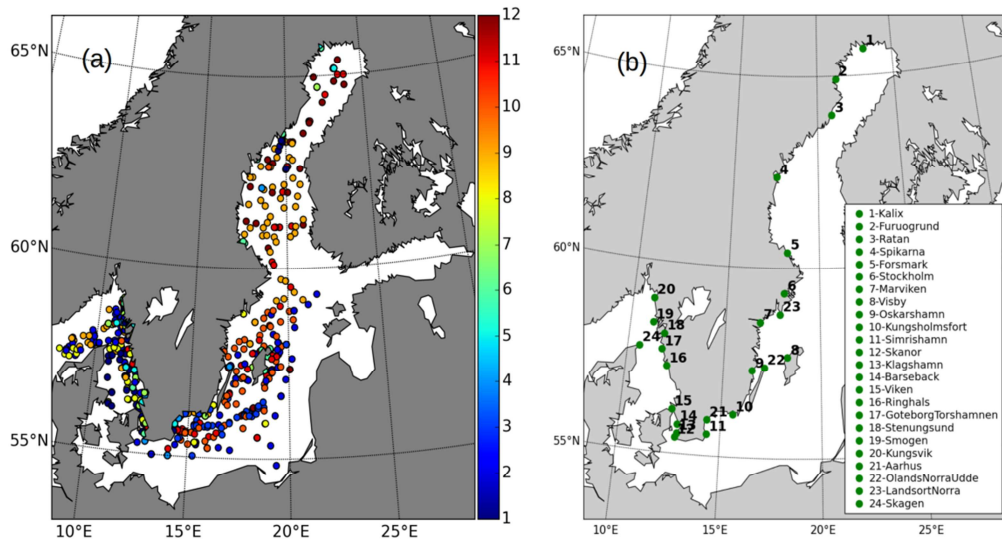
Figure 8. (a) Map of the temperature and salinity profiles from SHARK database in 2010. The colors

show the observations months.(b) The tide gauges station along the Swedish coast.

890

891

892

893

894

895

896

897

898

899

900

901

902
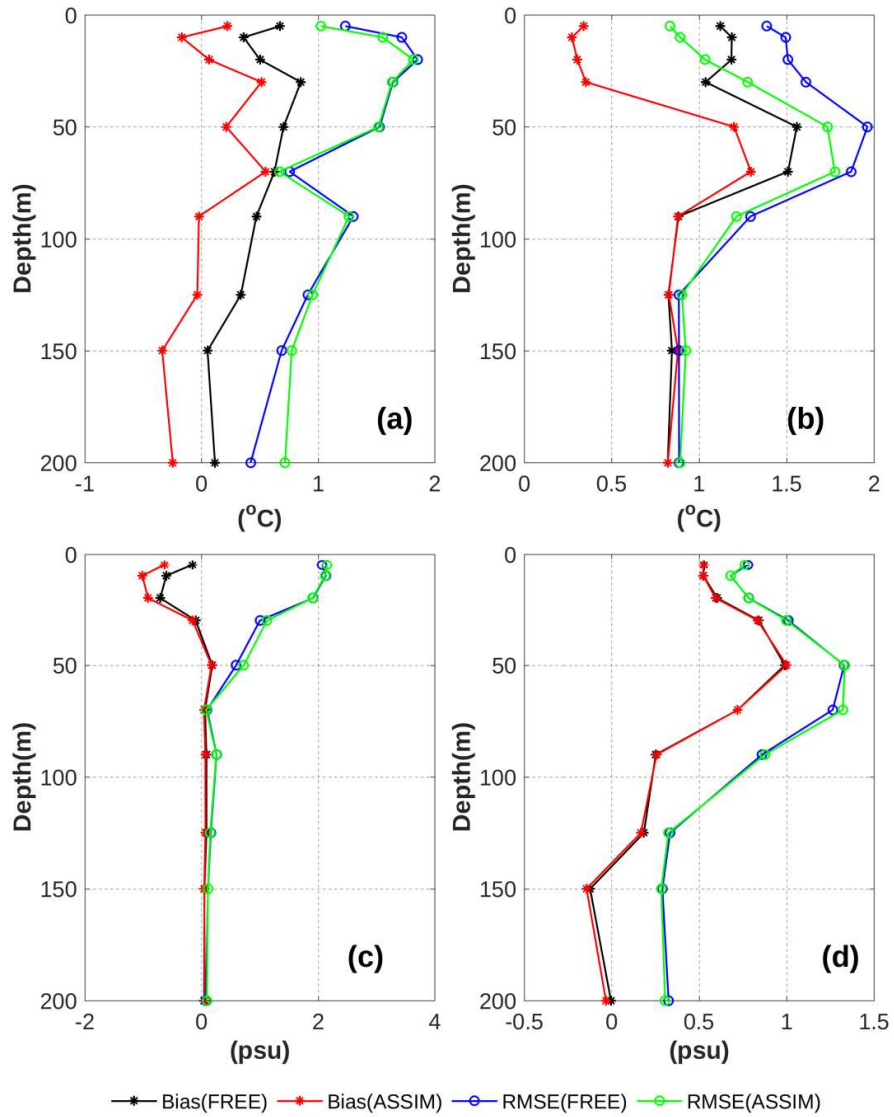
Figure 9. The overall RMSE and bias of temperature (up panel) and salinity (down panel) from FREE

and ASSIM relative to observations as a function of water depth inside (b,d) and outside (a,c) of the

Baltic Sea.

906

907

908

909
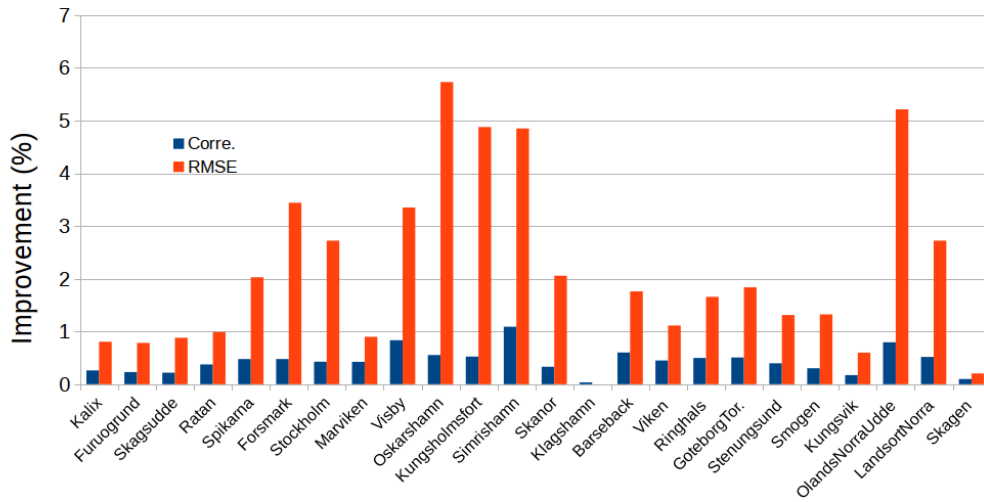
Figure 10. The improvement (%) of correlation and RMSE for the SLA at the tide gauges stations. The
station position is in the Figure 8b.
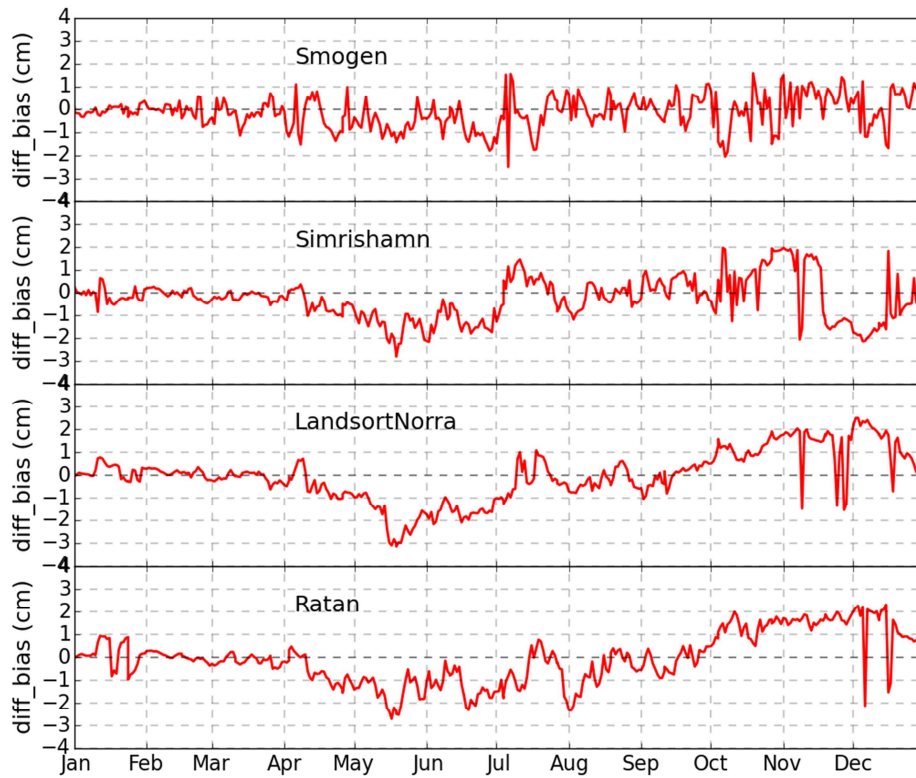
922

923   Figure 11. The variation of SLA biases in ASSIM relative to FREE against observations as a function

924   of time. The station position is shown in the Figure 8b.

925

926

927

928
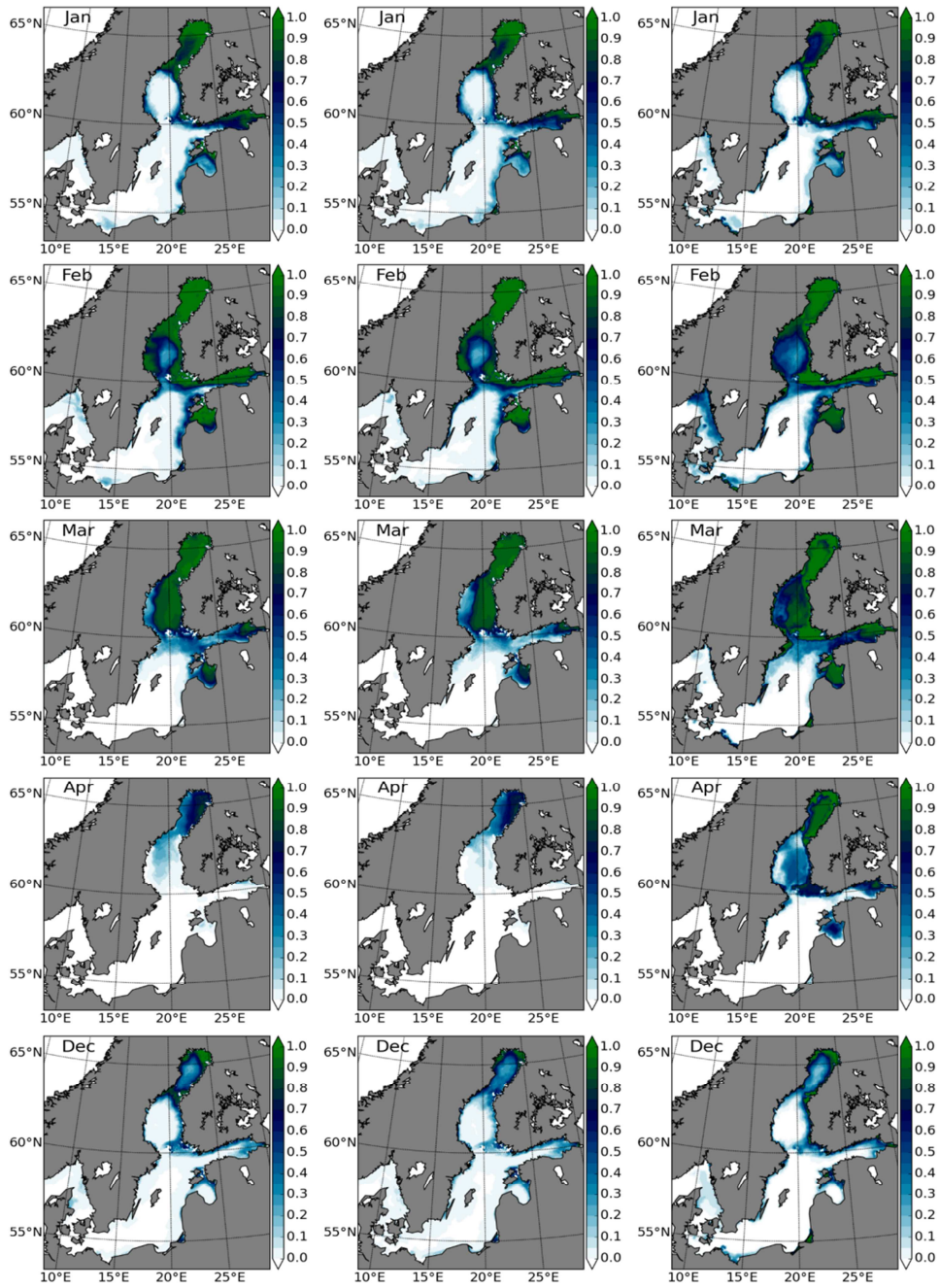
929

930   Figure 12. The monthly mean sea ice concentrations in FREE (left panel), ASSIM (middle panel) and

931   IceMap (right panel), respectively.

932

933

934
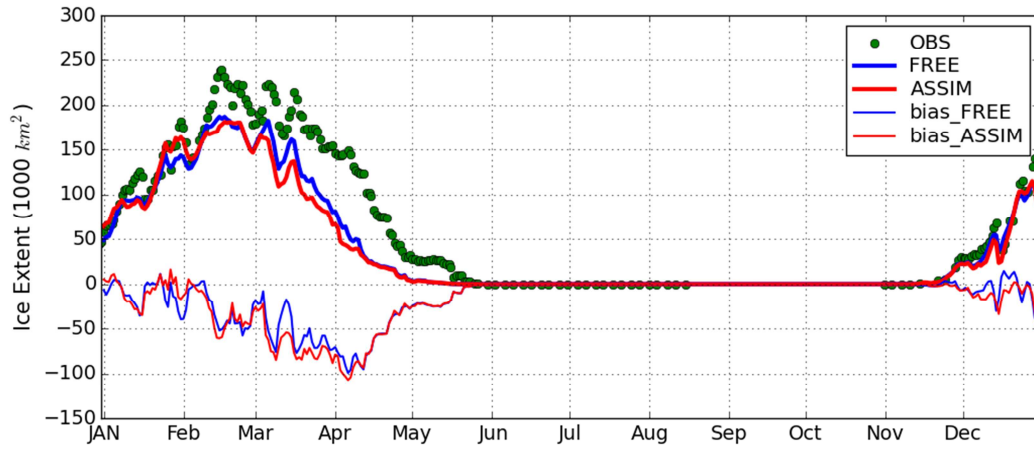
935

936   Figure 13. The daily sea ice extent from FREE, ASSIM and IceMap and the sea ice extent bias (mod-

937   elled minus observed field), respectively.

938